Characterization and Viscoelastic Modelling of a 3D Printed Conductive Polymer Metal Composite

A. Corke[1], I. Garces[1*], M. Biglarbegian[1]

[1] Mechanical and Aerospace Engineering, Carleton University, Ottawa, Ontario, Canada

* *Corresponding author (irinagarces@cunet.carleton.ca)*

Keywords: *Additive Manufacturing; Polymer-Metal Composite; Mechanical Characterization; Viscoelastic Modelling*

1. Abstract

Flexible electronics are increasingly important in wearable health monitoring, soft robotics, and structural monitoring where devices must conform to complex and often dynamic surfaces. Additive manufacturing of conductive thermoplastic composites enables rapid, customizable fabrication of such electronics without the need for dedicated tooling while offering the ability. However, these materials have inherent viscoelastic behaviours which remains poorly quantified yet critical to predicting electronic device performance. This work seeks to study the mechanical response of an extrusion based additively manufactured (EBAM) copper-reinforced thermoplastic composite through creep testing and evaluates the feasibility of using linear viscoelastic models to capture its strain response. Samples were mechanically conditioned to account for the inherent porosity of EBAM processed materials and subjected to creep testing at multiple stress levels with isochronous stress-strain curves constructed. Empirical linear viscoelastic models composed of Kelvin-Voigt Solid elements with a free damper and spring was developed based on the material's creep response. Conditioning reduced sample-to-sample variation, suggesting that initial differences were driven by manufacturing induced defects. All stress levels produced time-dependent strain, confirming viscoelastic behavior. Isochronous curves exhibited clear nonlinearity, indicating that the tested strain range exceeded the material's linear viscoelastic limit. The linear model fit the creep data well with increasing accuracy as additional elements were included, with marginal gains after 2 elements. However, residuals showed non-random structure, revealing model limitations, which when considered with the isochronous analysis findings, suggests that while the linear viscoelastic model performed well a nonlinear viscoelastic model would more accurately represent the material's generalized mechanical response.

2. Introduction

The development of thermoplastic composite materials for additive manufacturing (AM) has enabled fully additively manufactured application specific engineered components and devices. As a result, AM has increasingly been adopted across industry, including highly regulated sectors such as aerospace and medicine [1-4]. Composite thermoplastics allow for tailored mechanical properties and new functional capabilities. The incorporation of conductive materials, such as metallic and carbon-based reinforcements, has allowed for the development of AM electronics like circuits, sensors, and antennas [3-7]. Sensor fabrication is particularly promising as AM offers rapid low-cost fabrication of complex designs without the need for dedicated tooling [1]. Among AM methods, Extrusion Based Additive Manufacturing (EBAM) is widely used due to its reliability, simplicity, and the versatility of materials it can process, including thermoplastic composites [1], [6]. Conformal and flexible sensors produced through EBAM are especially valuable in robotics and healthcare, where devices must attach to non-planar and dynamic surfaces, and can allow for multi-material sensor integration within load bearing structures [6].

Recent studies have demonstrated the potential of EBAM fabricated sensors. Moeinnia et al developed a fully 3D printed capacitive pressure sensor array for prosthetics utilizing EBAM with carbon black reinforced thermoplastic polyurethane (TPU) for the dielectric elements and non-reinforced TPU for the structural elements [4]. Christ et al. designed a fully 3D-printed strain sensor based on TPU and multiwalled carbon nanotubes, using these materials achieving strong piezoresistive performance and reliability [8]. Guo et al. created a flexible tactile sensor capable of detecting human movements using EBAM of silver reinforced silicone elastomers [5].

Many of these studies rely on novel materials with limited mechanical characterization. Their deformation behaviour, cyclic response, and reliability under load remaining poorly quantified. These are essential for the modelling and optimization of AM components and devices. This challenge is compounded by the influence EBAM processing has on material performance. Compared to conventionally manufactured polymers, EBAM materials often exhibit anisotropic mechanical properties due to process induced variations in material distribution, interlayer fusion, density, and porosity in the form of internal voids [1], [9]. Unlike intentionally designed porosity (e.g. sparse infill), these voids introduce unintended changes in mechanical behaviour [9]. Combined with the inherent viscoelasticity of polymers, these variations complicate efforts to model and predict material response. Many AM sensors rely on mechanical inputs, where applied pressure induces strain to generate signals; however, viscoelastic materials exhibit rate-dependent and evolving responses under cyclic loading due to damage, permanent deformation, and void collapse, leading to signal drift. Because many AM sensors rely on mechanical deformation to generate signals, viscoelastic effects such as rate dependence, cyclic drift, and permanent deformation directly impact sensor performance. Thus, accurate mechanical modeling is critical for predicting sensor behavior and enabling design optimization without extensive experimental iteration.

Viscoelastic models can provide a framework for predicting the mechanical responses of thermoplastics [10]. Numerous studies have successfully modeled stress relaxation and creep in thermoplastics using both linear and non-linear viscoelastic models. Typically employing generalized models containing Maxwell or Kelvin-Voigt elements [11-14]. Historically, these models have been applied to unreinforced thermoplastics produced through conventional manufacturing [13–16], but recent work has expanded to reinforced composites [16], [17] and AM-fabricated materials [11], [18].

To support the design of AM sensors and electronics, it is essential to quantify the mechanical behavior of polymer-metal composites produced via EBAM. This study addresses this gap by characterizing the viscoelastic response of an EBAM manufactured metal-reinforced conductive thermoplastic and evaluating the feasibility of using linear viscoelastic models to create an empirical model that captures its static mechanical behavior.

3. Background

3.1. Isochronous Stress-Strain Behaviour

Identifying the linear viscoelastic range (LVR) of a polymer is necessary to accurately model a polymer's mechanical behaviour. Linearity is defined by the modulus response being independent of the applied stress [10]. Thus, the creep modulus (the ratio of strain to stress) at any time and any stress level must be identical as:

$$D(t) = \frac{\epsilon_a(t)}{\sigma_{0,a}} = \frac{\epsilon_b(t)}{\sigma_{0,b}} = \cdots = \frac{\epsilon_n(t)}{\sigma_{0,n}} \tag{1}$$

where creep modulus is represented by D, strain (ε), and stress (σ). One method for determining the LVR is to construct an isochronous stress-strain diagram of the material and to evaluate the isochronous variations of stress versus strain for linearity. This diagram is constructed by extracting the creep compliance of a material at constant times from multiple creep tests at different stress levels. If these isochronous points form a linear relationship at any given time, the material's mechanical behaviour can be modeled as linear over that strain range.

3.2. Generalized Kelvin-Voigt Solid Viscoelastic Model

The generalized Kelvin-Voigt Solid (KVS) linear viscoelastic model excels at modeling the creep behaviour of thermoplastic materials [10]. This model is composed of (KVS) elements in series with a free damper and a spring attached to the ends, as shown in Figure 1.

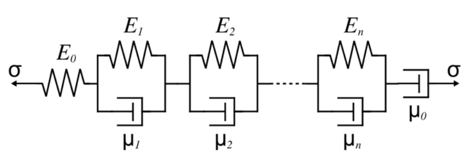

Figure 1. Generalized Kelvin-Voigt Solid Model.

The free damper captures potential permanent deformation while the free spring captures any instantaneous elastic behaviour. The elements within allow for fine tuning the models predicted viscoelastic behaviours, with the number of elements allowing for multiple relaxation times. Relaxation time (τ) being defined as the ratio of the dynamic viscosity (μ) to the elastic moduli (E) of the elements damper and spring, respectively. Creep compliance, *D(t)*, can be derived from this model to the form of:

$$D(t) = \frac{1}{E_0} + \sum_{i=1}^{n} \frac{1}{E_i}\left(1 - e^{\frac{-t}{\tau_i}}\right) + \frac{t}{E_0 \tau_0} \tag{2}$$

where E_0 represents the free springs modulus, τ_0 the free damper's relaxation time, and E_i and τ_i the individual element's modulus and relaxation time respectively. The strain of the material is found by applying the stress history (σ) to Equation 2, as:

$$\epsilon(t) = \sigma_0 \left(\frac{1}{E_0} + \sum_{i=1}^{n} \frac{1}{E_i} \left(1 - e^{\frac{-t}{\tau_i}} \right) + \frac{t}{E_0 \tau_0} \right) \tag{3}$$

4. Methods & Materials

4.1. Materials

A commercially available copper polyester-based thermoplastic was used for this study, Electrifi 3D Printer Conductive Filament (Electrifi, Multi3D, USA). The polymer is composed of three main components; copper flake reinforcements, polyester base, and processing aids. This combination was verified via a scanning electron microscopy on a printed sample. The resulting image shown in Figure 2 and the spectrum analysis averaged over each point and tabulated in Table 1. A composition of copper (reinforcement) at approximately 38% of the material, organic elements (polyester matrix) ~49%, and silver ~5% (processing aids) were verified.

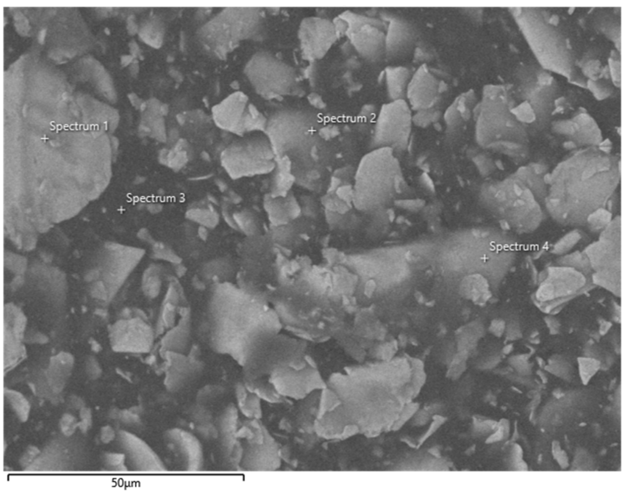

Figure 2. Scanning electron microscopy image of conductive thermoplastic composite 3D printed sample.

Table 1. Spectroscopy averaged analysis results.

Element	Line Type	Weight %
C	K Series	48.7 ± 0.3
O	K Series	8.6 ± 0.2
Cu	K Series	37.7 ± 0.3
Ag	L Series	5.1 ± 0.1

Table 2. Key printing parameters.

Parameter	Value
Nozzle Temperature:	160 °C
Line Width:	0.675 mm
Nozzle Diameter:	0.6 mm
Layer Height:	0.2 mm
Seam Position:	Randomized
Infill Percentage:	100 %
Infill Pattern:	Concentric
Maximum Volumetric Speed:	1.2 mm^3/s

4.2. Sample Manufacturing

Samples were designed as cubes with a nominal dimension of 5 mm in SolidWorks CAD (Dassault Group, France), then processed into G-Code format using Prusa Slicer (Prusa Research, Czech Republic). Samples were then manufactured using a Prusa XL 3D Printer (Prusa Research, Czech Republic) with a 0.6 mm nozzle. Manufacturer recommended printing parameters were used with the key parameters tabulated in Table 2.

4.3. Mechanical Testing

Loading was applied in uniaxial compression, normal to the samples printing layers using a TA Instruments ElectroForce DMA-3200. Preliminary testing revealed decreasing variation in strain responses between samples after repeat loading as expected from EBAM processed samples. Consequently, all samples were conditioned with static compressive loading prior to final testing. Conditioning loads were matched to the loads assigned for final testing. Samples were given at least 24 hours to elastically recover after conditioning before any further testing was done.

Creep tests were conducted at 1, 2, 4, and 6 MPa, with 7 samples tested at each level. Samples were loaded at a rate of 800 N/s and held for 500 s before being unloaded. Sample geometries were recorded before and after testing using a micrometer.

4.4. Isochronous Stress-Strain Analysis

Isochronous stress-strain curves were constructed using the strain and stress value from each sample at each creep testing level extracted at 50, 250, and 450 s as seen in Figure 1. The piecewise linear fitments were found using the Python library *pwlf* [19], which uses least squares regression to minimize the residuals of a continuous piecewise linear fitment. To assess the deviation between each segment's slope the percent difference was calculated using:

$$Percent\ Difference = \left(\frac{|m_p - m_c|}{\frac{m_p + m_c}{2}}\right) \cdot 100 \qquad (3)$$

where m_p represents the slope of previous segment and m_c the slope of the current segment.

4.5. Viscoelastic Model Fitting

Experimental data for each sample was fit to the generalized viscoelastic model with 0-3 KVS elements. The curve fitting was conducted using the python library *LMFit* [20], which minimizes the residuals of the fitment using the Levenberg-Marquardt algorithm. Initial guesses were adapted cyclically until a successful fitment was achieved. Best fit model parameters were then extracted and averaged within each creep test dataset. The R^2 value and the residuals were extracted for assessing the quality of the fitment.

5. Results and Discussion

5.1. Creep Testing

The conditioning process resulted in similar responses for all creep tests, as such a single representative conditioning process is shown in Figure 3. Engineering strain over time for the conditioning of samples tested at 6 MPa is shown in Figure 3a. The same data normalized to strain responses at a reference time of 30 s is shown in Figure 3b.

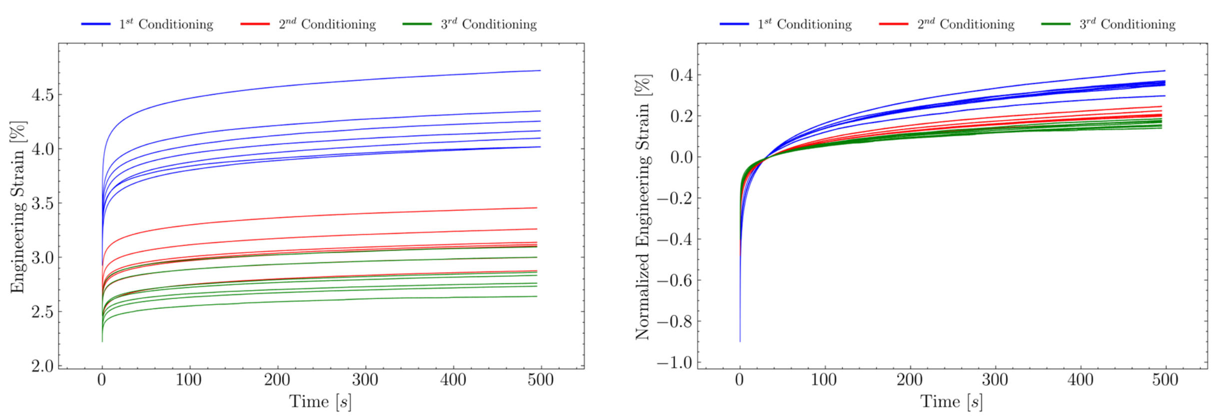

(a) Sample conditioning for 6 MPa samples

(b) Normalized engineering strain (30 seconds) versus time for 6 MPa sample conditioning

Figure 3. Conditioning data for 6 MPa samples.

Viscoelastic behaviour was observed with each sample showing increasing strain over time during static loading, hence demonstrating a time dependant relationship, which is as expected with viscoelastic behaviours commonly being reported for thermoplastics [10], [15], [17]. Within each conditioning test strain levels varied between samples. However, the shape of each curve remains similar, appearing as vertically shifted versions of each other. Subsequent conditioning tests show decreased variation in strain levels while maintaining the uniformity of response shape. Regarding Figure 3b with the normalized data, the first conditioning test displays higher strain levels over the same period with larger deviations in the strain response of each sample. The 2nd and 3rd conditioning tests appear to converge with lower overall strains compared to the first conditioning test. Each show limited deviations in strain levels between samples, and their strain response display near identical shape.

While absolute strains differ between samples, the shape of the materials strain response remained nearly identical. Suggesting that the differences seen in the strain response of the samples are due to sample specific conditions, such as manufacturing or testing variations, and not differences in material behaviour. This variation in strain response between conditioning cycles could be the effect of manufacturing defects introduced during the EBAM process. If internal voids are present, the stiffness of the sample would decrease, allowing for larger strains to occur. If these voids are collapsed permanently during loading the material would exhibit stiffening in its response to subsequent loadings, similar to what is being seen in these samples. This could be validated through quantification of the porosity of samples before and after testing. The material's stiffening between cycles should correlate with a decrease in porosity between conditioning cycles. As these voids continue to collapse a plateau should occur once all available voids are collapsed, creating a uniform strain response. This pattern is beginning to emerge, with the 2nd and 3rd conditioning cycles converge to similar strain magnitudes and response shape. Comparing EBAM prepared samples to those fabricated using convention methods could further validate this theory.

The measured creep data, engineering strain, is shown in Figure 4 as a function of time for all samples, with colours indicating the nominal stress level of the creep test, and vertical cyan dashed lines indicating isochrone times. Isochrone data was extracted from each creep test with the average strain and stress values from each time and creep test tabulated in Table 3.

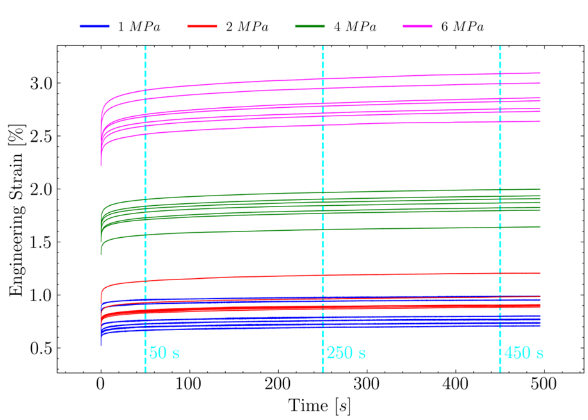

Figure 4. Engineering strain versus time for all creep testing.

Table 3. Creep testing isochrone data.

Test	Time [s]	Average Stress [MPa]	Average Strain [%]
1 MPa	50	0.976 ± 0.003	0.8 ± 0.1
	250	0.977 ± 0.006	0.8 ± 0.1
	450	0.976 ± 0.007	0.8 ± 0.1
2 MPa	50	1.78 ± 0.02	0.9 ± 0.1
	250	1.78 ± 0.02	0.9 ± 0.1
	450	1.78 ± 0.02	1.0 ± 0.1
4 MPa	50	3.67 ± 0.05	1.8 ± 0.1
	250	3.67 ± 0.05	1.8 ± 0.1
	450	3.68 ± 0.05	1.9 ± 0.1
6 MPa	50	5.59 ± 0.06	2.7 ± 0.1
	250	5.59 ± 0.06	2.8 ± 0.2
	450	5.59 ± 0.06	2.8 ± 0.2

It is clearly seen that larger stress loading results in larger strains and that each samples strain increases over time. This is a clear indicator of time dependent strain response and therefore viscoelastic behaviour. Sample variability in strain magnitudes is visible at all loading levels. The 1 MPa and 2 MPa creep tests have some overlap in sample strains, however when considering each test set as a group the median strains of the 2 MPa test remain higher, see Table 3.

5.2. Isochronous Stress-Strain Analysis

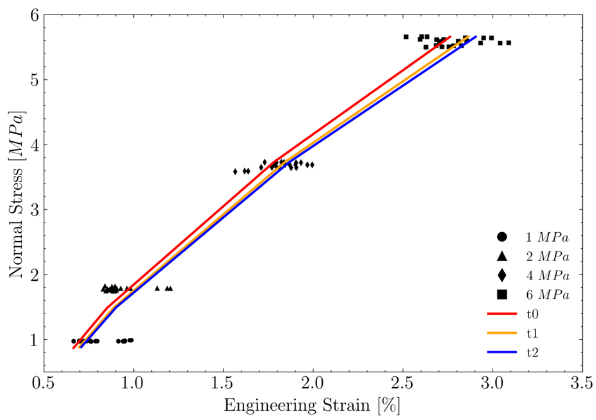

Figure 5. Isochronous stress-strain.

Table 4. Isochronous stress-strain curve fitment results.

Time	Segment	R^2	Slope	Percent Difference from Previous
50	1 - 2 MPa	0.972	3.30	-
	2 - 4 MPa		2.42	30.9 %
	4 - 6 MPa		1.97	20.5 %
250	1 - 2 MPa	0.972	3.14	-
	2 - 4 MPa		2.35	28.7 %
	4 - 6 MPa		1.89	21.6 %
450	1 - 2 MPa	0.973	3.15	-
	2 - 4 MPa		2.32	30.4 %
	4 - 6 MPa		1.86	22.0 %

Using extracted isochrones from the creep testing isochronous stress-strain curves were fitted for each time, with the resulting curves plotted in Figure 5. The slopes fitted between each creep test deviates between the segments, with each segment becoming shallower than the last. By calculating the percent difference between these slopes, see Table 4, it becomes clear that the slopes are changing substantially over these strain ranges with each curve showing over 20% change from the previous slope, thus indicating that the creep modulus is changing nonlinearly and outside its LVR.

The parameters extracted from each model fitment was averaged over each creep test dataset and tabulated in Table 5. All samples were successfully fitted to the data, however a few samples fitted to the 3-element model generated irrational values with extremely large errors and magnitudes. To not skew the averaged results these samples were removed from consideration in Table 5.

5.3. Viscoelastic Material Modeling

Best fit parameters from Table 5 across all elements and stress levels indicate the initial response (E_0) of the material exhibits a low modulus value ranging from 1.32 - 2.55 MPa. Subsequent moduli show significantly larger modulus values ranging from 21.7 – 52.6 MPa. This initial elastic response followed by stiffening over time is as expected for viscoelastic materials that exhibit time dependant relationship to strain. Conversely, relaxation times from the fitted models found the initial relaxation time, τ_0, to be significantly larger, with values ranging from 6122 – 28600 s, whereas all subsequent relaxation times ranged from 2.48 - 84.7 s.

Large relaxation times indicate terms that are non-dominate, the larger the value the longer it takes for the term to be fully realized and contribute to models' prediction of the material response. Thus, the regression analysis' large τ_0 value across all models suggests that the free damper term is non-dominate. Furthermore, as this term represents the free damper and therefore the permanent deformation it suggests that the materials response is not showing large permanent deformations. This is as expected, for the models were fitted to creep testing data only, which does not show any unloading periods which is where this deformation would be most visible.

Table 5. Kelvin-Voigt Solid linear viscoelastic model best fit parameters.

Nominal Stress [MPa]	KVS Branches	Minimal R^2	E_0 [MPa]	E_1 [MPa]	E_2 [MPa]	E_3 [MPa]	τ_0 [s]	τ_1 [s]	τ_2 [s]	τ_3 [s]
1	0	0.788	1.32054 ± 7E-5	-	-	-	7730 ± 10	-	-	-
	1	0.970	1.3840 ± 1E-4	21.68 ± 0.03	-	-	11510 ± 20	37.9 ± 0.1	-	-
	2	0.982	1.4239 ± 2E-4	26.90 ± 0.08	26.59 ± 0.06	-	24330 ± 60	13.39 ± 0.07	84.7 ± 0.3	-
	3*	0.985	1.4156 ± 6E-4	30.1 ± 0.2	32.4 ± 0.1	36.3 ± 0.2	19500 ± 200	2.48 ± 0.03	73.2 ± 0.6	37.0 ± 0.3
2	0	0.714	2.2620 ± 2E-4	-	-	-	6122 ± 9	-	-	-
	1	0.982	2.3895 ± 2E-4	29.27 ± 0.03	-	-	10390 ± 10	44.90 ± 0.09	-	-
	2	0.997	2.4015 ± 2E-4	33.37 ± 0.08	36.17 ± 0.04	-	13680 ± 50	53.4 ± 0.1	37.90 ± 0.06	-
	3*	0.997	2.4895 ± 5E-4	34.62 ± 0.09	41.92 ± 0.08	45.8 ± 0.01	28600 ± 900	70.9 ± 0.3	43.91 ± 0.08	6.44 ± 0.02
4	0	0.793	2.2870 ± 1E-4	-	-	-	7440 ± 10	-	-	-
	1	0.985	2.3995 ± 2E-4	36.15 ± 0.03	-	-	11020 ± 10	36.15 ± 0.07	-	-
	2	0.998	2.4857 ± 2E-4	45.12 ± 0.03	44.09 ± 0.04	-	13200 ± 10	50.09 ± 0.07	21.52 ± 0.03	-
	3	0.999	2.5468 ± 2E-4	55.02 ± 0.06	54.08 ± 0.07	51.38 ± 0.05	15320 ± 20	30.72 ± 0.05	32.88 ± 0.10	43.98 ± 0.06
6	0	0.811	2.2370 ± 1E-4	-	-	-	7220 ± 10	-	-	-
	1	0.984	2.3470 ± 2E-4	35.32 ± 0.03	-	-	10610 ± 10	36.53 ± 0.07	-	-
	2	0.997	2.4309 ± 2E-4	42.28 ± 0.04	43.28 ± 0.04	-	14260 ± 10	48.28 ± 0.05	32.74 ± 0.05	-
	3*	0.999	2.4723 ± 2E-4	48.08 ± 0.04	49.17 ± 0.05	52.60 ± 0.04	14620 ± 20	76.91 ± 0.09	33.64 ± 0.07	20.81 ± 0.03

*Outliers removed

Figure 6 shows a representative fitment for a single sample tested at 6 MPa with best fit curves for 0-3 KVS branches shown in (a) and the resulting residuals in (b). Experimental data is shown in black, with each model being represented by a different color. The model's ability to capture the material response improved with each added element, with marginal gains after 2 elements. This can be seen in the visual fitment of the best fit curves overlayed onto the experimental data shown in Figure 6a, in the increasing trend in minimal R^2 fitment approximations with each added element shown in Table 5, and by reviewing the residuals of each fitment shown in Figure 6b. With the magnitudes of the residuals decreasing with each added element. Inspecting the shape of the residuals it clearly displays a non-random pattern which deviates significantly at the beginning of the test and stabilizes as the test continues. This suggests the model is not perfectly capturing the material's response, particularly evident near the start where the elastic nature of the material dominates. Devore stipulates that difficulties such as these in nonlinear regression residual plots can indicate that the dependant and independent variables have a nonlinear relationship [21]. Considering the results of the isochronous stress-strain analysis which suggested that the material is outside its LVR, this non-random pattern could indicate that the material could be better modeled by a nonlinear viscoelastic model, particularly when predicting other mechanical responses such as relaxation or dynamic loading.

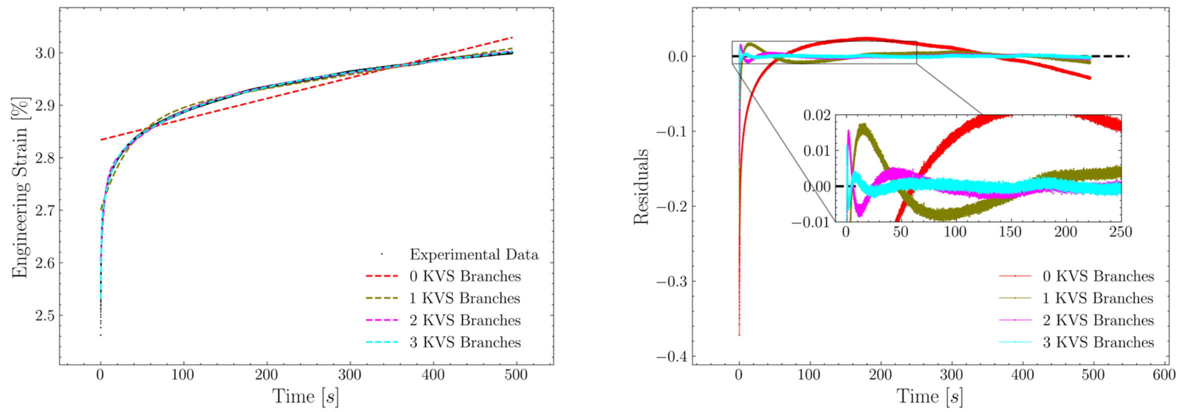

(a) Best fit curves for varying number of branches *(b) Fitted curve residual plots*

Figure 6. Representative KVS modeling plots for sample 5 at 6 MPa.

6. Conclusions and Future Work

A commercial conductive thermoplastic composite was mechanically conditioned and tested, revealing clear viscoelastic, time-dependent strain behavior. Initial conditioning cycles showed high variability in strain magnitudes, which decreased with repeated cycling, leading to more uniform responses. This variability is attributed to manufacturing induced defects (e.g., internal voids from EBAM), which are progressively reduced during conditioning. Isochronous analysis showed that stress–strain slopes varied significantly (over 20% between segments), indicating that the material operates outside the LVR for the tested strain levels (0.8–2.8%). Models with 2 and 3 KVS element models achieved strong agreement to creep data ($R^2 > 0.98$). However, residuals exhibited non-random patterns, suggesting potential model limitations when capturing other types of mechanical responses. Combined with isochronous results, suggests that a nonlinear viscoelastic model could better capture the material's response. The variation in strain magnitudes between samples should be further studied to definitively determine the source of the variation. The isochronous analysis could be expanded to include lower strain ranges to find the limits of the material's LVR, alternatively nonlinear viscoelastic models could be attempted to better model the materials mechanical responses. These refinements to the models' capabilities along with relating the strain response to electrical properties such as resistivity or permittivity would allow its use in predicting the behaviours and performance of any functional components manufactured with this and other similar materials.

Acknowledgments

The authors would like to acknowledge and thank La Fondation Dassault Systèmes for financially supporting this research. The authors would also like to thank Chantel Paquet and her team at the NRC for conducting the scanning electron microscopy testing.

References

[1] I. Gibson, D. Rosen, B. Stucker and M. Khorasani, *Additive Manufacturing Technologies,* 3rd ed. Cham Switzerland: Springer Cham, 2020.

[2] R. Striker, D. Mitra, B. D. Braaten, K. S. Kabir and S. Roy, "On the Manufacturing Process of a Single-Step Fully 3D Printed Conformal Patch Antenna," in *IEEE Int. Conf. on Electro Inf. Technol.*, 2020.

[3] P. Flowers, C. Reyes, Y. S, M. Kim and B. Wiley, "3D printing electronic components and circuits with conductive thermoplastic filament," *Additive Manuf.,* vol. 18, pp. 156-163, 2017.

[4] H. Moeinnia, D. J. Agron, C. Ganzert, L. Schubert and W. S. Kim, "Wireless pressure monitoring system utilizing a 3D-printed Origami pressure sensor array," *Flexible Electron.,* vol. 8, no. 1, p. 21, 2024.

[5] S.-Z. Guo, K. Qiu, F. Meng, S. H. Park and M. C. McAlpine, "3D Printed Stretchable Tactile Sensors," *Adv. Mater.,* vol. 29, 2017.

[6] M. J. Hossain, B. T. Tabatabaei, M. Kiki and J. W. Choi, "Additive Manufacturing of Sensors: A Comprehensive Review," *Int. J. of Precis. Eng. and Manuf.,* vol. 12, no. 1, pp. 277-300, 2025.

[7] N. Lazarus and H. Tsang, "3-D Printing Structural Electronics with Conductive Filaments," in *IEEE Trans. on Compon., Packag. and Manuf. Technol.*, 2020.

[8] J. F. Christ, N. Aliheidari, P. Pötschke and A. Ameli, "Bidirectional and Stretchable Piezoresistive Sensors Enabled by Multimaterial 3D Printing of Carbon Nanotube/Thermoplastic Polyurethane Nanocomposites," *Polymers,* vol. 11, no. 11, 2019.

[9] X. Sun, M. Mazur and C.-T. Cheng, "A review of void reduction strategies in material extrusion-based additive manufacturing," *Additive Manuf.,* vol. 67, 2023.

[10] H. F. Brinson and C. L. Brinson, *Polymer Engineering Science and Viscoelasticity: An Introduction*, 2nd ed., New York: Springer, 2015.

[11] J. Bochnia and S. Blasiak, "Stress Relaxation and Creep of a Polymer-Aluminum Composite Produced through Selective Laser Sintering," *Polymers,* vol. 12, no. 4, 2020.

[12] M. Schuster, K. Thiele and J. Schneider, "Investigations on the viscoelastic material behaviour and linearity limits of PVB," *CE Papers,* vol. 4, no. 6, 2021.

[13] J. Keursten, L. Kehrer and T. Böhlke, "Linear and nonlinear thermoviscoelastic behavior of polyamide 6," *Proc. in Appl. Math. and Mech.,* vol. 1, no. 22, 2023.

[14] T. Zink, L. Kehrer, V. Hirschberg, M. Wilhelm and T. Böhlke, "Nonlinear Schapery viscoelastic material model for thermoplastic polymers," *J. of Appl. Polym. Sci.,* vol. 139, no. 17, 2022.

[15] O. Starkova and A. Aniskevich, "Limits of linear viscoelastic behavior of polymers," *Mech. of Time-Dependent Mater.,* vol. 11, no. 2, pp. 111-126, 2007.

[16] S. Fliegener, J. Hohe and P. Gumbsch, "The creep behavior of long fiber reinforced thermoplastics examined by microstructural simulations," *Composites Sci. and Technol.,* vol. 131, pp. 1-11, 2016.

[17] Y. Qiu, J. Wang, D. Wu, Z. Wang, M. Zhang, Y. Yao and N. Wei, "Thermoplastic polyester elastomer nanocomposites filled with graphene: Mechanical and viscoelastic properties," *Composites Sci. and Technol.,* vol. 132, pp. 108-115, 2016.

[18] B. Adrover-Monserrat, S. García-Vilana, D. Sánchez-Molina, J. Llumà, R. Jerez-Mesa and J. A. Travieso-Rodriguez, "Viscoelastic Characterization of a Thermoplastic Elastomer Processed through Material Extrusion," *Polymers,* vol. 14, no. 14, 2022.

[19] C. F. Jekel and G. Venter, "pwlf: A Python Library for Fitting 1D Continuous Piecewise Linear Functions," (2019). Accessed: May 31, 2026. [Online]. Available: https://github.com/cjekel/piecewise_linear_fit_py

[20] M. Newville, S. T. A. D. and A. Ingargiola, *LMFIT: Non-Linear Least-Square Minimization and Curve-Fitting for Python. (*2014). Accessed: May 31, 2026. [Online]. Available: https://lmfit.github.io/lmfit-py/index.html

[21] J. Devore, *Probability and Statistics for Engineering and the Sciences*, 9 ed., Boston, MA: Cengage Learning, 2016.

[22] J. Pratama, S. I. Cahyono, S. Suyitno, M. A. Muflikhun, U. A. Salim, M. Mahardika and B. Arifvianto, "A review on reinforcement methods for polymeric materials processed using fused filament fabrication (FFF)," *Polymers,* vol. 13, no. 22, 2021.